The Journal of Chemical Physics

Rheology of *Pseudomonas fluorescens* biofilms: From experiments to predictive DPD mesoscopic modeling

Cite as: J. Chem. Phys. **158**, 074902 (2023); https://doi.org/10.1063/5.0131935
Submitted: 25 October 2022 • Accepted: 27 January 2023 • Accepted Manuscript Online: 30 January 2023 • Published Online: 16 February 2023

José Martín-Roca, Valentino Bianco, Francisco Alarcón, et al.

AIP Publishing

The Journal of Chemical Physics ARTICLE scitation.org/journal/jcp

Rheology of *Pseudomonas fluorescens* biofilms: From experiments to predictive DPD mesoscopic modeling

Cite as: J. Chem. Phys. 158, 074902 (2023); doi: 10.1063/5.0131935
Submitted: 25 October 2022 • Accepted: 27 January 2023 •
Published Online: 16 February 2023 • Corrected: 16 February 2023

José Martín-Roca,[1,2] Valentino Bianco,[2] Francisco Alarcón,[3] Ajay K. Monnappa,[4] Paolo Natale,[2,5] Francisco Monroy,[6,7] Belen Orgaz,[8] Ivan López-Montero,[2,5] and Chantal Valeriani[1,9,a)]

AFFILIATIONS

[1]Departamento de Estructrura de la Materia, Física Térmica y Electrónica, Universidad Complutense de Madrid, 28040 Madrid, Spain
[2]Departamento de Quimica Fisica, Universidad Complutense de Madrid, 28040 Madrid, Spain
[3]Departamento de Ingeniería Física, División de Ciencias e Ingenierías, Universidad de Guanajuato, Loma del Bosque 103, 37150 León, Mexico
[4]Instituto de Investigación Biomédica Hospital Doce de Octubre (imas12), 28041 Madrid, Spain
[5]Instituto de Investigación Sanitaria Hospital Doce de Octubre (imas12), 28041 Madrid, Spain
[6]Translational Biophysics. Instituto de Investigación Sanitaria Hospital Doce de Octubre (imas12), 28041 Madrid, Spain
[7]Biophysics for Biotechnology and Biomedicine (Biophys-HUB). Departamento de Química Física, Universidad Complutense de Madrid, 28040 Madrid, Spain
[8]Sección Departamental de Farmacia Galénica y Tecnología Alimentaria, Universidad Complutense de Madrid, Madrid, Spain
[9]Grupo Interdisciplinar Sistemas Complejos (GISC), Madrid, Spain

[a)]**Author to whom correspondence should be addressed:** cvaleriani@ucm.es

ABSTRACT

Bacterial biofilms mechanically behave as viscoelastic media consisting of micron-sized bacteria cross-linked to a self-produced network of extracellular polymeric substances (EPSs) embedded in water. Structural principles for numerical modeling aim at describing mesoscopic viscoelasticity without losing details on the underlying interactions existing in wide regimes of deformation under hydrodynamic stress. Here, we approach the computational challenge to model bacterial biofilms for predictive mechanics *in silico* under variable stress conditions. Up-to-date models are not entirely satisfactory due to the plethora of parameters required to make them functioning under the effects of stress. As guided by the structural depiction gained in a previous work with *Pseudomonas fluorescens* [Jara *et al.*, Front. Microbiol. 11, 588884 (2021)], we propose a mechanical modeling by means of Dissipative Particle Dynamics (DPD), which captures the essentials of topological and compositional interactions between bacterial particles and cross-linked EPS-embedding under imposed shear. The *P. fluorescens* biofilms have been modeled under mechanical stress mimicking shear stresses as undergone *in vitro*. The predictive capacity for mechanical features in DPD-simulated biofilms has been investigated by varying the externally imposed field of shear strain at variable amplitude and frequency. The parametric map of essential biofilm ingredients has been explored by making the rheological responses to emerge among conservative mesoscopic interactions and frictional dissipation in the underlying microscale. The proposed coarse grained DPD simulation qualitatively catches the rheology of the *P. fluorescens* biofilm over several decades of dynamic scaling.

I. INTRODUCTION

Bacterial biofilms are synergistic colonies growing on solid surfaces in contact with a complex aqueous phase that provides physical protection against external threats.[1,2] Because biofilm colonies are mechanically more resilient than the isolated bacteria, they become more capable to nurse resistant phenotypes.[3,4] A collective efficiency emerges from the microbial colony to engender antibiotic

resistances and compromise substrate removal, hence causing persistent biofilm infection.[3,4] Surface biofilm formation is indeed a major health issue[5,6] and an industrial challenge worldwide.[7–9] The mesoscopic structure of biofilms consists of a flexible meshwork made of bacteria and extracellular polymer substance, which is composed of polysaccharides, proteins, and extracellular DNA embedded in aqueous suspension. Depending on the bacterial species, the amount of thriving cells with respect to the EPS vary from one tenth to one fourth of the total biofilm mass.[10] Biofilms are considered to be complex materials as highly cross-linked EPS composites with a heterogeneous viscoelasticity acting as a dynamic scaffold for dwelling cells.[11,12] Recently, biofilm viscoelasticity has been considered for probing the mechanical interlinking between EPS components and dwelling bacteria.[12–17] For a complexity emerging from compositional and topological configurations in the EPS assembly at multiple length scales,[13,18,19] biofilms exhibit both elasticity and fluid-like rheological response upon shear arising from their complex hydrodynamic dependence on deformation amplitudes and frequencies.[14–17] Relevant structural interactions, such as bacterial entanglement, protein binding, and EPS cross-linking, contribute to form the transient stress-bearing structure that makes the particular biofilms' viscoelasticity to emerge from the mesoscale.[20–22] Recent structural studies have shown that EPS constituents, such as secreted polysaccharides, DNA chains, and other protein filaments, biochemically dictate matrix architecture and biofilm stability under low mechanical load in the linear regime.[20–22] However, there is a lack of understanding of the cross-linking, dynamical rearrangements, and mesoscopic reorganizations under large shear forces mimicking real-thing perturbations. Rheological techniques for probing large-amplitude shear deformation have allowed us to record rheological signatures at a variety of stresses under wide configurational landscape[12,14,16,17,23] and strong history fidelity (i.e., presenting viscoelastic memory).[15] The biofilms grown under different mechanical conditions are indeed known to exhibit viscoelastic variations corresponding to environmental adaptations.[12,24] Furthermore, EPS viscoelasticity is known to confer protection against chemical and physical threats.[1,25] While ample literature alludes to the biomolecular role of the EPS secreted under stressed biofilm growth,[1,12,24] systematic investigations of the rheological response are still lacking on the biophysical focus. To investigate *in silico* a synthetic rheology of biofilms that further improves our predictive ability from structural coarse-grain standpoints, we invoke numerical modeling from mesoscopic physics as approached alongside experimental rheology data obtained in physicochemically controlled biofilms.[15]

Physical biofilm modeling started more than one decade ago in terms of continuous media approaches.[26,27] They were first described via phase-field (continuum) models in which the disperse phase accounts for polymerized biofilm components (EPS and bacteria) and the continuous phase accounts for aqueous ambiance (containing nutrients and many other small molecules).[28] This model has been successfully used to recapitulate essentials of biofilm growth, particularly unraveling mechanical features in agarose hydrogels containing bacteria.[29] A further approach consisted in implementing hybrid discrete–continuum models to couple bacterial growth and biomass spreading over biofilm roughness.[30,31] Numerical mesoscale approaches have also been proposed, particularly Dissipative Particle Dynamics (DPD[32,33]) and the Immersed Boundary-based Method (IBM).[34,35] IBM relies on strong assumptions, such as (a) considering biofilm steadiness during the simulation time scale,[36] (b) imposing biofilm elasticity as linear springs connecting individual bacteria,[37] and (c) capturing the biofilm viscosity via constitutive stresses. Encoding these constraints has allowed for using IBM for studying biofilm growth and its force-guided deformation,[38–41] establishing connections between mechanical stress and biofilm strain.[36,37,42] The DPD methods are comparatively less astringent in mechanical terms than IBMs.[43] Indeed, DPD is a mass and momentum conserving algorithm that allows us to model many-bodies embedded in a viscous fluid,[32,33,44] even when geometries are complex.[45,46] *Quasi*-continuous DPD-approaches have been indeed revealed with a predictive capacity in describing certain rheological features of *Staphylococcus epidermidis* biofilms grown on a rheometer plate.[47,48] By running DPD-simulations over long time and length scales,[43] the method has also been used to simulate biofilm formation on post-coated surfaces[40] and the growth of two-dimensional biofilms under external flow.[45]

More recently, some of us worked on a combined numerical and experimental study aimed at unraveling how hydrodynamic stress globally affects the mechanical features of *Pseudomonas fluorescens* biofilms.[12] The *P. fluorescens* biofilms were grown under either static or shaken conditions. Rheological measurements combined with confocal microscopy were further performed on real biofilms. The experimental results showed the cultured *P. fluorescens* biofilms as capable of adapting to environmental conditions by tailoring their matrix microstructure to mechanical stress.[12] By considering prospective DPD simulations allowing us to define the mesoscopic framework recapitulating principal ingredients from real biofilm behavior [polymer density, cross-linking degree, number of bacteria, etc.], those previous results suggested DPD-based rheological modeling with a forecasting potential. In particular, DPD-simulations showed how much structural change was caused by an increased number of cross-links in the EPS matrix.[12] In exploring the mechanical DPD-landscape as led by the living bacteria, however, the parameter space of the DPD method was not fully mapped, and more importantly, the viscoelastic behavior of the biofilm to the applied shear frequencies was not studied in the time domain.

Beyond our previous work,[12] we here exploit novel coarse-grained DPD-modeling to numerically map rheological biofilm features in mechano-structural landscapes exploring nonlinear dynamic stress responses. The parameter space of biofilm viscoelasticity has been now mapped varying both mesh topology and structural compositions as represented by bonding interactions, such as the number of cross-links between EPS polymers, the number of embedded bacteria, and the biofilm swelling amount of water molecules interacting along the DPD field. In order to check for dynamic (conservative/dissipative) features as structurally connected with the underlying biofilm mechanics, the rheological DPD-response has been now explored in the time domain under variable strain spanning a broad range of shear amplitudes (both in linear and nonlinear regimes). The viscoelasticity predicted by the DPD-method has been further subject to experimental validation by measuring *in situ* responses of real *P. fluorescens* biofilms grown under either mild static conditions or intense shear stimuli. As a novel piece of retrospective physical forecasting on biofilm

dynamics, our experimental findings with *P. fluorescens* biofilms have been discussed in the sight of the numerical outcomes obtained from new DPD-simulations.

This paper is organized as follows. We first describe the formal DPD-framework, its numerical setup, and the validating experimental methods. Section III comprises an ample setting of numerical DPD simulations mapping a broad rheological space at variable stress in two differentiated cross-linking topologies, either tightly (compact) or sparsely (homogeneous) cross-linked. The simulation results are then discussed on the sight of the experimental evidence accumulated on the *P. fluorescens* biofilm rheology,[12] including new viscoelasticity measurements obtained at variable frequency under extreme conditions of growing, either statically unstressed or under shaking stresses. Finally, we summarize the conclusions.

II. NUMERICAL AND EXPERIMENTAL METHODS

We first present the novel mesoscopic DPD-method used to simulate *in silico* the differently formed *P. fluorescens* biofilms subject to variable shear stress spanning from *quasi*-static up to shaken conditions mimicking biofilm formation under hydrodynamic stress. Synthetic biofilms are prepared at periodic boundary configuration consisting of a colony of monodisperse bacteria immersed in a simulation box containing randomly distributed polymers and solvents. We also describe the experimental rationale designed for rheological measurements in biological biofilms at retrospective correspondence with simulations on synthetic biofilms.

A. Mesoscopic DPD-simulations

A given biofilm is modeled *in silico* as a mesoscopic system of interacting beads recapitulating the three different components: bacteria, polymers, and water. First having built a polymer matrix as a mesh of rigid bonds with a fixed cross-linking, we randomly insert monodisperse-sized bacteria and finally hydrate the entire system with water molecules. While Raos *et al.*[49] dispersed the single bacterium as filler spherical particles, we build here rod-shaped bacteria by aggregating 440 simulation beads, each one with diameter σ_b, then brought together via harmonic spring interactions,

$$U_b^{\text{bond}} = \frac{K_b}{2}(r_{i,j} - \sigma_b)^2, \tag{1}$$

with $r_{i,j}$ being the distance between bonded beads i and j and K_b being the harmonic coupling constant. The bacterium body is formed as a spherocylinder whose central part is shaped as an empty cylinder of length $l_b/\sigma_b = 6$, while the extremes of the bacteria are shaped as spherical caps of radius $R_{ext}/\sigma_b = 4$. Both the central and extreme parts have an external radius $R_{ext}/\sigma_b = 4$ and internal radius $R_{\text{int}}/\sigma_b = 2$, i.e., the bacterium membrane is formed by three layers of particles.

These rigid bacteria are immersed in a flexible mesh made of polymers (EPS) hydrated with water molecules. Water is represented by N_{solv} bead particles of type s. The EPS matrix consists of linear chains of l beads bounded via an harmonic potential,

$$U_p^{\text{bond}} = \frac{K_p}{2}(r_{i,j} - \sigma_p)^2, \tag{2}$$

where $r_{i,j}$ is the distance between two consecutive beads i and j, σ_p is the equilibrium distance, and K_p is the coupling constant. The polymer beads of type p can cross-link each other and with neighboring bacteria (bacterium–polymer cross-links). These cross-linking (CL) interactions have also been represented as harmonic potentials, as established in Eqs. (1) and (2). Using the above structural approach, all the bounding interactions are encoded inside the mesoscopic simulation box, namely, polymer–polymer (pp), polymer–bacterium (pb), polymer–solvent (ps), bacterium–bacterium (bb), bacterium–solvent (bs), and solvent–solvent (ss).

Within the current simulation DPD-schema, the total force between two particles i and j consists of three interactions: conservative, dissipative, and random. The sum of the three DPD components captures long-range correlations induced by hydrodynamic interactions and also accounts for thermal fluctuations. The net force between two particles i and j (of types α and β) can be expressed as the sum of the conservative force $\vec{F}_{i,j}^{C}$ plus the dissipative force $\vec{F}_{i,j}^{D}$ and the random force $\vec{F}_{i,j}^{R}$. The conservative force corresponds to $\vec{F}_{i,j}^{C} = B_{\alpha,\beta} w(r) \hat{r}_{i,j}$ for $r < r_c$, where r_c is a cut-off distance beyond which all these terms vanish; $\hat{r}_{i,j}$ is the unit vector along the direction of $\vec{r}_i - \vec{r}_j$, indicating the positions of particles i and j, respectively; and $B_{\alpha,\beta}$ is the amplitude of the conservative force between particles of types α and β. The dissipative force is represented as $\vec{F}_{i,j}^{D} = -\gamma w^2(r)(\hat{r}_{i,j} \cdot \hat{v}_{i,j})\hat{r}_{i,j}$, where $\vec{v}_{i,j} \equiv \vec{v}_i - \vec{v}_j$ is the vector difference between the velocity $\vec{v}_i$ of particles i and the velocity $\vec{v}_j$ of particle j. Here, γ is the friction coefficient. The random force can be computed as $\vec{F}_{i,j}^{R} = w(r)\left(\frac{2k_B T\gamma}{dt}\right)^{1/2} \Theta \ \hat{r}_{i,j}$, $w(r) = 1 - r/r_c$, being $w(r)$ a weighting factor varying from 0 to 1. Θ is a Gaussian random noise with zero mean and unit variance, dt is the integration time, k_B is the Boltzmann constant, and T is the absolute temperature. This random force essentially captures the microscopic Newtonian friction as balanced against the fluctuating impulsion by the thermal energy transferred from the environment.

By using internal units, we set $r_c = 1$ for all DPD interactions, $\sigma_b = \sigma_p = 0.5$, $\gamma = 4.5$, and $K_b = K_p = 30$. The time step is set to $dt = 0.05$ although we test our results also against $dt = 0.005$. To convert dimensionless units in physical units, we consider $k_B T = 4.11 \times 10^{-21}$ J as the characteristic energy scale, and we set the length scale to the longest dimension of one *P. fluorescens* bacterium, ~1.5 μm. Since the size of one bacterium is about 1.5 μm and one bacterium os about 10 beads long, the diameter of one bead (σ_b) corresponds to about 100 nm. Having assumed $\sigma_b = \sigma_p$, the size of a single polymer in the experiments (about 100 nm) would correspond to a single bead. For this reason, in our simulations, we assume that polymer chains inserted in the system represent a network of connected polymers, comparable in size with the bacteria. Moreover, since the mass of a single bacterium is $\sim 10^{-15}$ kg, the mass of a single particle is set to $m_u \sim 2.3 \times 10^{-18}$ kg. The time scale is derived accordingly as $\tau_{\text{intrinsic}} = \sqrt{m_u l_u^2 / k_B T} \sim 5 \times 10^{-6}$ s.

B. Synthetic biofilm: Simulation scheme

We prepare configurations of bulky 32 × 32 × 32 biofilm boxes, which are evolved in time via a constant-volume DPD dynamics performed using an open source Large-scale Atomic/Molecular

Massively Parallel Simulator (LAMMPS)-integrator package imposing periodic boundary conditions.[50] To study rheological features, the parameter space is explored as follows: a number of bacteria N_b ranging from 100 to 200, a number of polymers N_p ranging from 80 to 200 (of polymer lengths $L_p = 100$), and a number of solvent particles N_s ranging from 20 000 to 50 000. All parameters N_p, N_s, and N_b have been chosen to fulfill the DPD condition for the density;[32,51] this is $(N_p + N_b + N_s)/(32 \times 32 \times 32) > 3$. To guarantee bacteria and polymers being properly hydrated, we choose the amplitudes of the solvent interactions smaller than any others. In particular, we choose $B_{s,s} = B_{s,b} = B_{s,p} = 25$ and $B_{b,b} = B_{p,p} = B_{p,b} = 30$. When varying the water content, to study the effect on the rheology when changing the biofilm solvation, we accordingly changed N_b and N_p to always keep the overall system's density larger than 3.

In order to understand whether our polymer suspension is in a dilute or semi-dilute regime, we compute the average polymer concentration of our simulations and relate it to the overlap concentration. We estimate the polymer overlap concentration as $c^* \sim N_p/L_p^3$, where N_p is the number of monomers in one polymer and L_p is the polymer length. In a theta-solvent, we can approximate $L_p \sim N_p$, leading to $c^* \sim 1/N_p^2 = 0.0001$ (being $N_p \sim 100$). Given that we insert about 100 polymers, each one of length 100, the average polymer concentration is about 0.3, which is above the overlap concentration. Thus, we are dealing with a semi-dilute polymer system.

To prepare initial configurations, we randomly locate N_b bacteria and N_p polymers in the presence of N_s water molecules and then equilibrate without polymer cross-links (CLs) for $\sim 8 \times 10^6$ time steps. Next, we turn on the cross-links within the polymer network. For any choice of N_b and N_p, we form a fixed number of cross-links ranging from 2300 up to 5400. To create the network of cross-linked polymers and bacteria, we randomly place N_{CL} newly formed harmonic bonds (1) between b and p particles, i.e., bacterium–polymer cross-links, and (2) between two p particles belonging or not to the same polymer chain, i.e., polymer–polymer cross-links. To avoid the formation of artificial aggregates of p particles, we forbid cross-links between nearest-neighbor beads belonging to the same polymer chain. Thus, we choose, on the one hand, to inhibit cross-links between the ten closest neighboring particles belonging to the same chain. The resulting homogeneous topology is referred to as T_A (with a probability for each chain monomer to cross-link $p_A = 1/10$). On the other hand, we choose to allow for cross-links between particles that are more than three neighbors apart. We refer to the resulting polymer compact topology as T_B (with a threefold higher cross-linking probability than T_A, i.e., $p_B = 1/3 > p_A$). Unless specified otherwise, all the presented results will refer to the topology T_A, considered to be sufficiently open to allow for bacterial reorganizations. To prevent excess formation of cross-links per particle, which would result in a globule-like cluster of particles, we assume that any particle of type b can form at most one cross-link, while any p particle can form at most two cross-links. After cross-link formation, a second equilibration run of $\sim 10^6$ time steps is performed to relax the polymer–bacterium network.

Figure 1 shows an example of an equilibrated configuration corresponding to the homogeneous T_A topology considered undeformed (in the absence of shear stress).

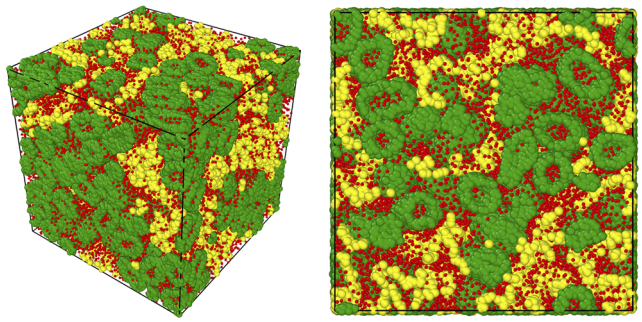

FIG. 1. Synthetic DPD-biofilms in the homogeneous T_A topology: Left panel: simulated structure after numerical equilibration. Snapshot of the simulation box containing 184 bacteria (in green), 80 polymers (in yellow), and 35 000 solvent particles (in red). Right panel: cross section of the same system.

C. Canonical T_A topology: Pair distribution function

As expected, the homogeneous T_A–biofilm is characterized by an homogeneous distribution of bacteria within a weakly cross-linked matrix as characterized by the radial distribution function $g_{b-b}(r)$ computed on the center of mass of bacteria [Fig. 2(a)].

All the radial distribution plots exhibit a marked peak corresponding to nearest-neighbor correlations at short distances $r/\sigma \sim 5$, while approaching $g_{b-b}(r) \sim 1$ at longer distances, as expected in homogeneous liquids. Regardless of the number of bacteria N_b, the number of polymers N_p, the number of cross-links, and the level of hydration N_s, all curves representing $g_{b-b}(r)$ show exactly the same behavior [differently colored curves in Fig. 2(a)]. As representative configurations, the blue and red curves reported in Fig. 2(a) refer to systems with different CL numbers, whereas the green and blue curves refer to systems that differ in N_b, CL, and N_s.

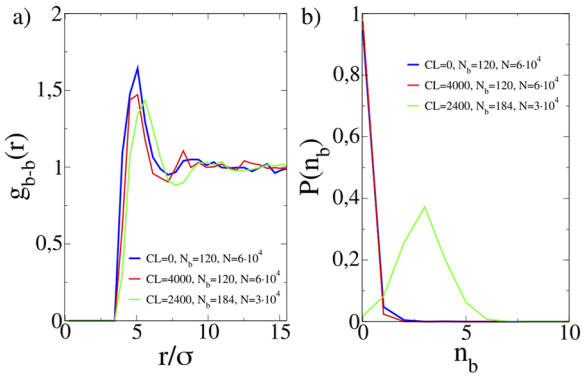

FIG. 2. (a) Radial pair distribution function for the center of mass of bacteria for three sets of parameters: CL = 0, $N_b = 120$, $N_p = 80$, $L_p = 100$, $N_s = 60\,000$ (blue); CL = 2400, $N_b = 184$, $N_p = 80$, $L_p = 100$, $N_s = 30\,000$ (green); and CL = 4000, $N_b = 120$, $N_p = 80$, $L_p = 100$, $N_s = 60\,000$ (red). (b) Probability distribution function for the number of bacteria in box slices of size $L/4$ [system parameters as in (a)].

In order to test the occurrence of bacterial aggregation in the initial sample, we look for the appearance of phase separation (which would result in clustering of bacteria). For this purpose, we compute the density distribution of the center of mass of bacteria, shown in Fig. 2(b). To perform this calculation, we divide the box volume in cubic cells of size $L/4$ and compute the number of bacteria per cell. Finally, the distribution is computed over multiple cells taken from several independent configurations. The blue and red curves refer to systems with a lower number of bacteria, resulting in averaging mostly empty cells, while the green curve refers to a system with a larger number of bacteria, resulting in a non-vanishing average density. Independent of the number of bacteria N_b, of polymers N_p, of cross-links, and of the level of hydration N_s, we observe a single-peak distribution. This underlines the fact that the system is locally structured but not phase separated (in agreement with the expected biofilm homogeneity in the weakly cross-linked T_A topology). Even though the snapshots in Fig. 1 seem to suggest that biofilms are spatially inhomogeneous, neither of the two procedures (TA or TB, data not shown) lead to a phase separated system. Work is in progress to build a model characterized by a clear spatial inhomogeneity, based on a combination of polymers of different lengths, together with a biased bacterial aggregation.

For a fixed number of bacteria, polymers, and water content, we have estimated the average distance between two connected beads in the polymer mesh and demonstrated that it is a decreasing function of the total number of cross-links, as expected. Since the larger the total number of cross-links, the larger the number of cross-links between polymers and the smaller the average distance between two connected beads in the polymer mesh. When the number of cross-links is larger than 2000, the average distance between two connected beads in the polymer mesh does not vary considerably (data not shown). Throughout the rest of this work, we will only consider a biofilm matrix in the T_A topology and with a number of cross-links larger than 2000.

D. Numerical DPD-rheology

To study the rheological properties of a given model biofilm, we compute the shear modulus by monitoring the shear stress response $\sigma_{xy}(t)$ resulting from an imposed sinusoidal deformation of the simulation box.[12,43] We apply an external oscillatory shear deformation with time frequency ν along the X–Y plane by changing the box size L according to

$$L(t) = L_0 + A\,\sin(2\pi\nu t), \tag{3}$$

with $L_0 = 32$ being the initial box size and A being the oscillation's amplitude. According to Raos *et al.*,[49] the resulting stress can be calculated by fitting the xy component of the shear stress with

$$\sigma_{xy}(t) = \sigma' \cdot \sin(2\pi\nu t) + \sigma'' \cdot \cos(2\pi\nu t), \tag{4}$$

with σ' and σ'' corresponding to the in-phase and out-of-phase components of the complex shear modulus G, whose components are

$$G' = \frac{\sigma'}{(A/L_0)}, \qquad G'' = \frac{\sigma''}{(A/L_0)}, \tag{5}$$

with G' being the storage modulus and G'' being the loss modulus, respectively. Whereas rheological properties of solids are characterized by a finite storage modulus $(G' > 0)$, fluid viscous materials are characterized by near zero storage $(G' \sim 0)$ and large losses $(G'' > 0)$.[3,52,53]

When shearing the DPD-system, we choose to vary the amplitude A between 4 and 36 corresponding to a maximal deformation strain $(u = A/L_0)$ of up to the 112% of the box size. We mainly focus on data obtained for $A = 24$ $(u = 75\%)$ since the stress–strain curve behaves almost linear nearby but departs from linearity for larger deformations. We herein find the response stronger and the noise lower when varying system parameters (N_b, N_p, ...). Under shearing conditions, particle velocities are remapped every time they cross periodic boundaries.

Having performed preliminary numerical experiments with a simulation box of $16 \times 16 \times 16$, we obtained the same rheological behavior as with a larger system of $32 \times 32 \times 32$. Therefore, we chose the larger box to study the bulk rheological features of a bacterial biofilm. We choose a period $T \equiv \frac{2\pi}{\nu}$ ranging between 2×10 up to 2×10^5. At a time step of $dt = 0.01$, a period of $T = 200$ corresponds to 2000 time steps that is within the total lifespan of the simulation runs. For the considered frequency, ranging from a value of 3×10^{-5} to a value of 0.3 (in internal units), we run simulations completing at least three box-shearing oscillations. Once numerical simulations of shearing have been performed in internal units, the rheological results can be converted into physical units by multiplying the shear stresses inside the simulation box into physical pressures in each XY-plane wherein the shear strain is a constant. For the considered simulations, the conversion factor is $N_{XY} m_u/(l_u \tau_u) = 4.1$ kPa per internal unit of pressure as considered in each shear plane containing $N_{XY} = 32 \times 32 = 1024$ particles.

E. Viscoelasticity regimes

As a rule of thumb on the proposed DPD-rheology, we performed simulations in synthetic biofilms with an intermediate number of particles interacting in rigid realizations under dominant chain cross-linking in the canonical T_A topology. Figure 3 shows typical stress–strain plots obtained for the considered medium and high cross-linking (respectively, CL = 3600, 5300) and extremal values of the shear frequency.

From a phenomenological point of view, the computed stresses are characterized by two regimes with the dependence of the applied strain on the synthetic DPD-biofilms $(u = A/L_0)$, which imposes the stress response on the dependence of the prescribed degree of cross-linking in simulated topologies.

On the one hand, for the in-phase stresses, we detect the following [Fig. 3(a)]: (a) a Hookean elastic regime at low strain below a strengthening point $(u < u_{st})$ [here, stress and strain are linearly related until the onset for dynamic rigidization (nearby u_{st})] and (b) a nonlinear regime beyond the strengthening point $(u > u_{st})$ [here, the system strengthens under nonlinear stress, thus becoming effectively stiffer than in the Hookean regime]. Very relevantly, the higher the number of cross-links, the strengthener the resulting synthetic biofilms. As expected, for rigid networks made of semi-flexible polymers with permanent cross-links,[54] the most rigid synthetic realization arises from the densest cross-linked mesh strained at the highest frequency (at short deformation period $T = 200$).

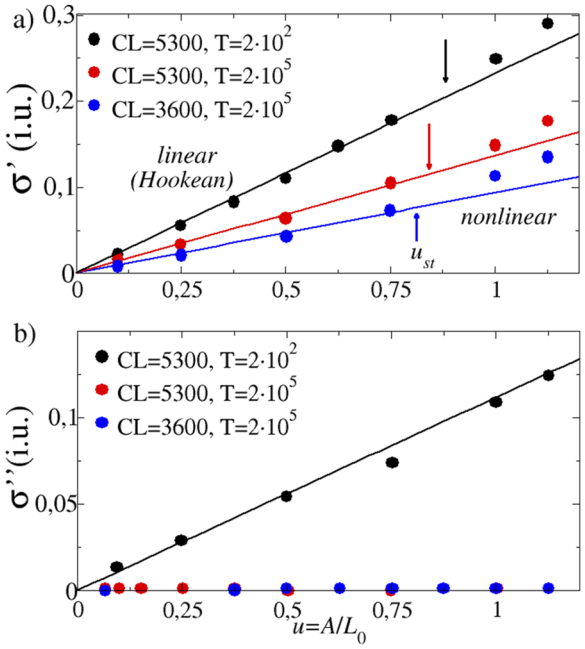

FIG. 3. Rheological DPD-response of synthetic biofilms. In-plane stress σ' (a) and σ'' (b) as a function of A/L_0 for three different biofilms characterized by 5300 cross-links and $T = 200$ (black symbols), 5300 cross-links and $T = 2 \times 10^5$ (red symbols), and 3600 cross-links and $T = 2 \times 10^5$ (blue symbols). The straight lines are needed to underline the regime where we consider the shear to be linear. All data refer to $N_b = 150$, $N_p = 80$, and $N_s = 45\,000$.

On the other hand, the out-of-phase stresses show the viscous losses as a dissipative frictional response [Fig. 3(b)]. The presence of finite (non-zero) viscous shear stresses is only detected for the most rigid realizations with the highest density of cross-links strained at high frequency (black symbols); viscous stress is detected neither at low frequency (red symbols) nor at low density of cross-links (blue symbols). Therefore, we identify the densely cross-linked as a viscoelastic material. Whereas a high systemic shear rigidity makes the elastic response to emerge solid-like ($\sigma' \sim G'u$ with $G' \gg 0$), the finite dynamic viscosity imposed by the DPD algorithm makes the frictional losses to effectively emerge only at high frequency (i.e., $\sigma'' \sim G''u$ being $G'' = \omega\eta$ the loss modulus as determined by the shear viscosity η). Otherwise, the synthetic system behaves inviscid ($\sigma'' \sim 0$).

F. *In vitro* biofilm formation

Strain *P. fluorescens* B52, originally isolated from raw milk,[55] is used as a model micro-organism. Overnight, precultures and cultures are incubated at 20 °C under continuous orbital shaking (80 rpm) in tubes containing 10 ml Trypticase Soy Broth (TSB, Oxoid). Cells are recovered by centrifugation at 4000 g for 10 min (Rotor SA-600; Sorvall RC-5B-Refrigerated Superspeed Centrifuge, DuPont Instruments) and washed twice with a sterile medium. Cellular suspensions at OD_{600} are first adjusted to 0.12 (equivalent to 10^8 cfu/ml) and then diluted to start the experiments at 10^4 cfu/ml. Biofilms are grown on borosilicate glass surfaces (20×20 cm^2) as adhesion substrates. Five glass plates are held vertically into the sections of a tempered glass separating chamber, provided with a lid. The whole system is heat-sterilized as a unit before aseptically introducing 2 ml of the inoculated culture medium. To check the effect of hydrodynamic stress on biofilm mechanical properties, incubation is carried out for 96 h at 20 °C both in an orbital shaker at 80 rpm (shaken sample) and statically (non-shaken sample). For biofilm recovery, plates are aseptically withdrawn, rinsed with sterile saline to eliminate weakly attached cells, and then scraped to remove the attached biomass (cells + matrix) from both sides of the plates. For rheological measurements, the biofilm material is casted every 24 h to be directly poured onto the rheometer plate. Experiments are run in triplicate.

G. Experimental rheology

The biofilm's viscoelastic response is experimentally determined in a hybrid rheometer under oscillatory shear stress-control (Discovery HR-2, TA Instruments) using a cone-plate geometry (40 mm diameter) and a Peltier element to control temperature.[12] Triplicate measurements are performed at a 1 mm gap between the Peltier surface and the cone-plate tool (TA instruments), where a sinusoidal shear strain $u(t)$ of amplitude u_0 is performed at a frequency $\omega = 2\pi\nu$, i.e., $u(t) = u_0 \sin(\omega t)$. The shear deformations are considered at variable angular frequency ($\omega = 2\pi\nu$). The lower frequencies are restricted by the extremely long readout times compromising sample stability ($\nu_{\min} = 10^{-2}$ Hz). The practicable frequency window is upper limited by inertia ($\nu_{\max} = 100$ Hz); higher oscillation frequencies are not usually considered to be affected by artifacts in a blind region dominated by inertia. Measurements are performed at low strain amplitudes (typically $A = 1\%$), for which the stress responses are found practically linear. The shear stress exerted by the biofilm in the linear regime is monitored as $\sigma(t) = G^* u(t)$, where G^* is the viscoelastic modulus $G^* = G' + iG''$. The storage modulus accounts for Hookean shear rigidity ($G' \sim G_0$), and the loss modulus accounts for Newtonian viscous friction ($G'' = \eta\omega$; at constant shear viscosity η).

III. RESULTS

Our numerical simulations focus on mechanical measurements covering linear and nonlinear regimes of predictive viscoelasticity in synthetic DPD-biofilms. As guided by preliminary simulations performed to determine the viscoelasticity regimes (see Fig. 3), we build upon our numerical setup for the near-conservative DPD-rheology by keeping fixed $N_b = 150$, $N_p = 80$, and $N_s = 45\,000$ (corresponding to a well-populated biofilm colony). Hereinafter, all data refer to a low frequency deformation that minimizes the frictional losses (at period $T = 2 \times 10^5$). Simulation runs were performed as a function of the shear amplitude $u = A/L_0$ for different numbers of polymer–polymer or polymer–bacterium cross-links with topology either T_A or T_B. The DPD-realizations here performed actually correspond to relatively lower degrees of cross-linking as above considered in Fig. 3. They should capture the fuzzy structure expected for realistic EPS-networks in which the embedded particles are able to explore an ample configurational space even under relatively small amplitudes of the shear field externally applied.

A. Synthetic mechanical response under increasing shear deformation: Influence of biofilm topology

In order to characterize the parameter space of dynamical responses to shear corresponding to the considered cross-linking topologies (T_A and T_B), we compute the mechanical stress as a function of the shear strain for biofilms as those prepared in Sec. II (keeping fixed $N_b = 150$, $N_p = 80$, $T = 2 \times 10^5$, $l = 100$, and the total number of cross-links $CL_{pp} + CL_{pb} = 1600$). The results from these DPD-simulations are reported in Fig. 4 (symbols corresponding to systemically different DPD-realizations). The elastic (in-phase) stress shows a Hookean limit of the linear response at low shear deformations ($u = u_C \sim 50\%$), followed by a nonlinear trend toward higher stresses at larger deformations ($u \gg 75\%$). Differences appear when looking at the magnitude of G' when considering biofilms containing cross-links between particles within the same polymer chain. If they are more than three neighbors apart as in the compact T_B topology, the biofilm is always more rigid (Fig. 4; hollow symbols) than when containing cross-links between particles that are at least ten neighbors apart, i.e., the homogeneous topology T_A (solid symbols). The performed DPD-simulations show that cross-links between particles that are closer along the same polymer chain lead to stiffer biofilms: this might be the consequence of aggregation induced in the polymer chains. Under shear strain, the data become clearly grouped corresponding to the studied topologies; they are T_A: the structurally homogeneous T_A-topology, showing low stress and a broad linear regime under deformation, and T_B: the structurally compact T_B-topology, much stiffer, hence responding to higher stresses and ampler non-linearity. We superpose parabolic fits as straight lines to indicate the amplitude range where we can consider the quadratic shear response as limited by the leading Hookean component. The viscous (out-of-phase) stresses remain practically vanishing in these settings, which behave practically frictionless ($\sigma'' \sim 0$; data not shown). In both topologies T_A and T_B sheared under large amplitude deformation ($u \geq u_{st}$), the current DPD-simulations evidence nonlinear strengthening without increasing frictional losses due to conservative elongational chain ordering templated between the permanent cross-links of a rigid meshwork.

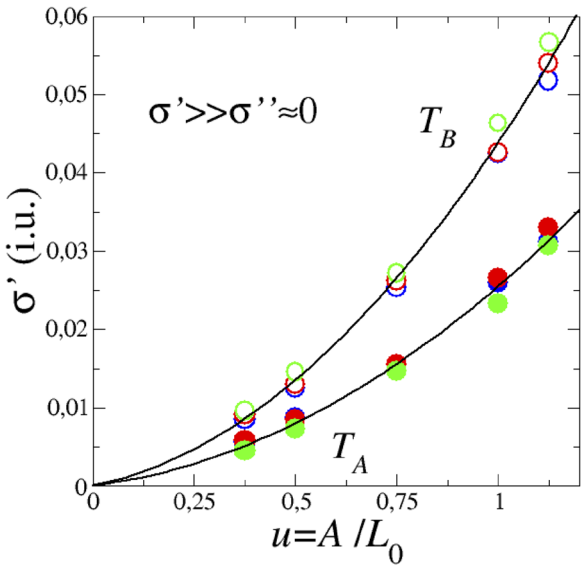

FIG. 4. Conservative shear response of synthetic DPD-biofilms under shear strain. The in-phase stress σ' is represented as a function of A/L_0 for three different biofilms each characterized by a different topology: T_A (solid circles) and T_B (hollow circles), in internal unit (i.u.). The color code indicates different numbers of polymer–polymer (pp), polymer–bacterium (pb) cross-links: $CL_{pp} = 200/CL_{pb} = 1400$ (blue); $CL_{pp} = 400/CL_{pb} = 1200$ (red); and $CL_{pp} = 600/CL_{pb} = 1000$ (green). All data refer to $N_b = 150$, $N_p = 80$, $N_s = 45\,000$, and $T = 2 \times 10^5$. The straight lines represent parabolic fits to simulation data (see the main text).

Different from our previous experimental results with *P. fluorescens* biofilms[12] and unlike rheological biofilm data reporting on nonlinear softening, e.g., in *S. epidermis*, *S. mutans*, etc. (see Ref. 15 for a review), the permanent cross-linking considered by our DPD-simulations predicts biofilm hardening as expected for polymer chains becoming rigidly ordered under stress. Such classes of strengthening stresses have been observed in modified biofilms composed of variants of *P. aeruginosa* able to overproduce rigid EPS polysaccharides.[56] This confirms that our "stiff" DPD-simulation framework is too rigid to capture collective relaxations from mobile cross-links and sliding entanglements as existing in the real biofilms. Despite these obvious limitations, we resume our analysis on the possibilities, capacities, and strengths of the current DPD-simulation schema based on permanent cross-links.

B. Effective (linear and nonlinear) shear rigidity

We further calculate the effective rigidness of the studied DPD-biofilms defined as the apparent modulus for elastic storage, i.e., $G' = \sigma'/u$ [see Eq. (5), left]. This effective parameter measures the apparent rigidity as recapitulated in a shear modulus for elastic storage. To calculate the effective rigidity as a function of strain $G'(u)$, we use raw simulation data on the stress–strain response (Fig. 4). Figure 5 plots simulation data for the apparent storage modulus G' increasing non-linearly with the shear amplitude (found larger in magnitude for the stiffest T_B biofilm than for the canonical T_A topology). The linear rigidity modulus is given by the Hookean limiting intercept at zero-strain (G_0 at $u = 0$).

The effective storage modulus increases with the strain-amplitude in both topologies (being larger in magnitude for the more compact T_B). This is the sort of behavior expected for semiflexible networks undergoing stress strengthening as simulated here.[54] We observe in both cases that the shear rigidity is not too much affected by the ratio between polymer–polymer (pp) and polymer–bacterium (pb) cross-links as long as the total number of CL remains constant in simulations. To calculate the Hookean moduli (G_0) and the nonlinear amplitudes (g_1), we exploit the phenomenological dependency $G' = \sigma'/u \sim G_0 + g_1 u + \cdots$ (see linear fits in Fig. 5). The fitting parameters are collected in Table I.

In both topologies (T_A and T_B), we compute the Hookean moduli with values around $G_0 \sim 0.01 \sim 1$ kPa (corresponding to a simulation box with $N = 32\,768$ particles inside); they estimate the mechanical rigidness of the synthetic biofilms in qualitative agreement with previous experiments performed with the *P. fluorescens* biofilms studied in the linear rheological regime.[12] The fitted values found for the nonlinear amplitudes g_1's reveal strong biofilm

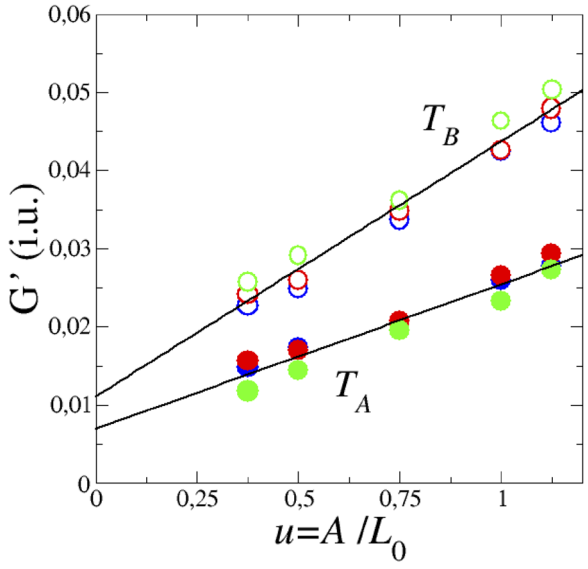

FIG. 5. Storage modulus G' as a function of strain for the topologies T_A (filled squares) and T_B (empty circles) in internal unit (i.u.). The color code indicates different numbers of polymer–polymer (pp), polymer–bacterium (pb) cross-links: $CL_{pp} = 200/CL_{pb} = 1400$ (blue); $CL_{pp} = 400/CL_{pb} = 1200$ (red); and $CL_{pp} = 600/CL_{pb} = 1000$ (green). All data refer to $N_b = 150$, $N_p = 80$, $N_s = 45\,000$, and $T = 2 \times 10^5$. The straight lines represent linear fits to simulation data (see the main text).

strengthening under stress, which is however not observed in the experimental window explored in the previous paper.[12] The current simulations show the effective DPD-rigidities increasing by more than 100% for T_A and 300% for T_B (considered both at 100% strain, i.e., at $u = 1$; see Fig. 5). Interestingly, the rigidness ratios indicate the relative softness of the homogeneous topology T_A with respect to the compact one T_B, i.e., $G_0^{(A)}/G_0^{(B)} \sim g_1^{(A)}/g_1^{(B)} \sim 0.6$. These mechanical ratios are hopefully determined by structural cross-linking probabilities relative to both simulated topologies, i.e., $1 - p_A/p_B \sim 0.6$, as encoded in the DPD-method (see Sec. II). Therefore, and in order to accommodate enough structural flexibility in the DPD-biofilms numerically simulated in the following, we will only deal with the homogeneous mesh works modeled at inhibiting cross-links between the ten closest neighboring particles belonging to the same chain (canonical T_A topology).

TABLE I. Characteristic parameters of shear rigidity calculated from the storage modulus in the studied DPD-topologies. G_0 is the Hookean shear rigidity, and g_1 is the nonlinear amplitude that describes biofilm strengthening under stress. The internal unit (i.u.) of rigidness can be converted into physical units of pressure by the factor 1 int. stress unit $= N_{XY} m_u/(l_u \tau_u) = 4.1$ kPa for $N_{XY} = 32 \times 32$ particles in each shear plane.

	G_0 (i.u.)	g_1 (i.u.)
T_A	0.007 ± 0.001	0.019 ± 0.001
T_B	0.011 ± 0.001	0.033 ± 0.002

C. Tuning structural parameters into synthetic DPD-modeled biofilm viscoelasticity

To analyze how far structural parameters, such as N_b, N_p, and N_s, affect biofilm viscoelasticity, we consider the homogeneous DPD-biofilms created with the canonical T_A cross-linking topology (i.e., by inhibiting cross-links between the ten closest neighbors in a polymer chain). We study stress responses from those flexible T_A biofilms designed to be a flexible meshwork within a dissipative dynamics (see Sec. II for details on DPD simulations). Figure 6 shows the dependence of the mechanical properties on N_b, N_p, and N_s as implemented in the canonical T_A topology. We set an intermediate number of cross-links ($CL = 2300$) and intermediate values of $N_p = 80$, $l_p = 100$, and $N_s = 35\,000$ within the explored range. Having prepared a DPD-biofilm with an equilibrated T_A topology, we apply a deformation amplitude of $A = 75\%$ and a deformation period of $T = 200$, both comprised well within a viscoelastic response entering the onset of nonlinearity. Significantly, we aim at mapping the effective response of the simulated DPD-biofilms in broad ranges of rheological behavior, making the compositional effects to emerge in the apparent viscoelastic moduli G' and G'' [as calculated from Eq. (5)]. These choices on the T_A topology are dictated by the fact that they correspond to a significant response of G'' as we have observed at high frequency, differently from the vanishing losses as happening at lower frequencies. Three different structural biofilm variations will be relevantly considered as referred to changes in the number of bacteria (N_b), of polymer matrix cross-links (N_p), and of water (solvent) molecules constituting the aqueous environment (N_s). These constitutional effects are discussed below.

Bacterial content. To check whether the shear stress depends on the number of bacterial cells (N_b), we have computed G' (in-phase response to strain) and G'' (out-of-phase response) as a function of N_b while keeping all other parameters fixed [Figs. 6(a) and 6(d)]. On the one hand, simulations show that the in-phase response (accounting for the storage modulus G') remains constant throughout the N_b range [Fig. 6(a)]. This result is in agreement with previously reported data.[11,15] By considering the bacterial biofilm as a polymer–colloid viscoelastic medium,[11,13–17] G' should increase with the density of bacteria until reaching a solid-like plateau. Our simulation data point out that the probed N_b-range falls into the elastic response regime where G' is not affected by N_b [Fig. 6(a)]. On the other hand, the loss modulus G'' linearly increases with N_b [Fig. 6(d)], reflecting the high friction imposed on the cross-linked mesh by dragging large bacterial objects while increasing density. In agreement with a solid-like behavior lead by the rigidity of the cross-linked mesh, G'' is always smaller than G' but approaches larger values compatible with the storage modulus for the largest number of bacteria hereby considered. We conclude, therefore, about simulated biofilm behavior as a viscoelastic material with a relatively high structural rigidity dominant over viscous fluidity (i.e., $G' > G''$). Otherwise stated, our model predicts the rheological behavior of a quite resilient material with a relatively high mechanical compliance.

Polymer density. To check the effect of an increasing number of cross-linked polymers on the shear response, we set $N_b = 150$, $l_p = 100$, $N_s = 35\,000$, and $CL = 2300$ with an amplitude of $A = 75\%$ and a period of the deformation of $T = 200$ [Figs. 6(b) and 6(e)]. When increasing the number of polymers keeping a constant bacterial density, we observe the simulated biofilm to engender a

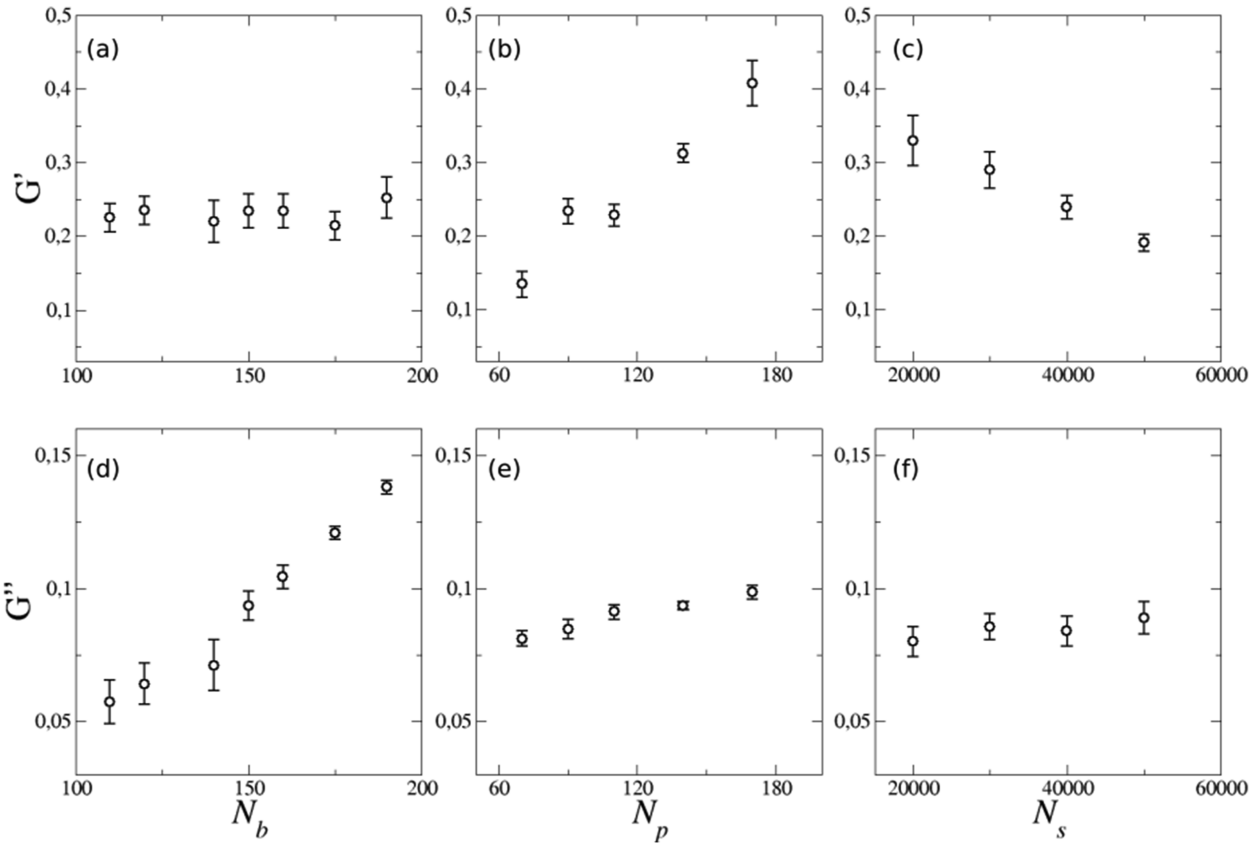

FIG. 6. Stress components G' and G'' for $A = 75\%$, $CL = 2300$, and $T = 200$ as a function of (a) and (d) the number of bacteria N_b and (b) and (e) the number of polymers N_p and solvents (c) and (f).

solid-like network with an increasing rigidity with increasing mesh density [Fig. 6(b)]. This suggests that bacteria can colonize a pre-existing polymer mesh and modify its rigidity according to their space needs; the denser template could entail the more bacteria in a stiffer mesh. However, the out-phase stress response increases only slightly by increasing the number of polymers [Fig. 6(e)]. Since an increase of the number of polymers corresponds to a small increase in G'' when compared to the response originated by bacteria [Fig. 6(d)], we conclude that G'' is almost independent of the polymer concentration as corresponding to our essentially rigid DPD-system to describe mesoscopically unrelaxed chains within the permanent cross-links considered. As referred to the predominantly solid-like behavior emerged with increasing bacterial numbers [N_b in Figs. 6(a) and 6(d)], the present results also evidence how biofilm rigidity can be enhanced by increasing polymer numbers [N_p in Figs. 6(b) and 6(e)]. These simulations on the compaction effects induced by polymer density essentially reproduce the nonlinear rheological characteristics experimentally observed for bacterial biofilms of single species with a well-structured EPS (i.e., macroscopically homogeneous, compact, and continuous).[15]

Solvent effects. Furthermore, mechanical responses were tested for different hydration levels ($CL = 2300$, $N_b = 184$, $N_p = 80$, and $l_p = 100$). Upon biofilm deformations of high amplitude ($A = 75\%$) and long period ($T = 200$), we observe a hydration effect that makes the storage modulus to decrease with the number of solvent particles [Fig. 6(c)] and preserves regulated friction losses [Fig. 6(f)]. Our biofilm DPD-model seems to be able to absorb the water molecules to mechanically soften at near constant viscosity. Such nonlinear softening emerges as far as averaged distances between bacteria and polymers largely increase by solvent dilution under intense shear deformation, thus making the network to become mechanically softer.[15] Mesh weakening is however not reflected in the loss modulus because DPD only catches the viscosity of the solvent but not collectively mesoscopic relaxations.

D. Rheological dependence on the shear frequency: Experiment vs simulation

We performed rheological experiments on *P. fluorescens* biofilms grown upon both static and shaken culture conditions

(see Sec. II G). The viscoelastic responses were subject to dynamic scrutiny under oscillatory shear deformation fixed in the linear regime ($A = 1\%$) and variable frequency in the experimentally available window from $\nu = 0.01$ Hz up to ~100 Hz ($\nu = \omega/2\pi$). Figure 7 compares experimental results (upper panel) and DPD-simulations as performed at equivalent time units (lower panel). The *P. fluorescens* biofilms have both been grown for 24 h: the first one under static culture conditions [Fig. 7(a); red symbols] and the other one under shaking [Fig. 7(a); black symbols]. Immediately after culture, we place the grown biofilm *ex vivo* in the rheometer and then measure both the linear response G' (solid symbols) and G'' (hollow symbols), either for the static biofilm (red symbols) and for the shaking biofilm (black symbols). Due to the technical limitations of the used rheometer, we underline that we could not measure the stress moduli of the *P. fluorescens* biofilm grown under shaking conditions for frequencies beyond 100 Hz established as a practical ceiling value for experimental macro-rheology. The recorded data intentionally correspond to the linear regime of viscoelastic response ($A = 1\%$) in which a quasi-static response is expected at compatibility with the permanent nature of the rigid (passive) cross-links considered in simulations. Further active effects present in the real biofilms as nonlinear softening stresses ($A \geq 10\%$),[12] reconfigurable cross-links, or propulsion bacterium impulses are not discussed here as not being explicitly considered in the current DPD-simulations only capturing quasi-static interactions between "passive" biofilm components in a fixed meshwork of permanent cross-links.

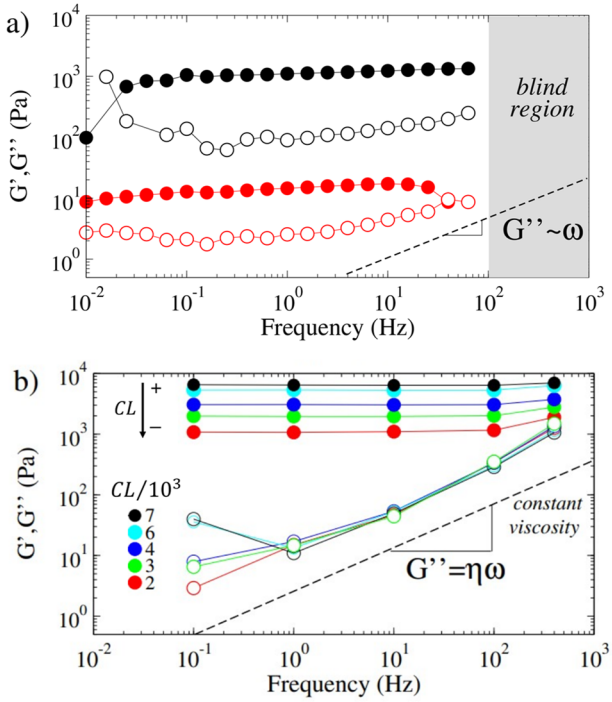

FIG. 7. (a) Experimental measurements of the elastic modulus (G'; solid symbols) and loss modulus (G''; hollow symbols) for two different classes of *P. fluorescens* biofilms: The rigid one grown under shaking conditions (black) and the softer one obtained under static conditions (red), measurements performed in triplicate. The symbols represent averaged data replicated in each condition (experimental reproducibility compatible with symbol size). The near constant storage moduli evidence soft solid behavior ($G' \sim G_0$). The dashed line indicates the Newtonian trend expected at high frequency for the loss modulus under dominant viscous friction ($G'' \sim \omega$). The gray shadowed blind region is not accessible to experiments (see Sec. II G). (b) Synthetic rheology in DPD-biofilms with a variable number of permanent cross-links at the T_A-topology: G' (solid symbols) and G'' (hollow symbols) computed for the biofilm model. Data refer to $N_b = 184$, $N_p = 80$, $l = 100$, $N_s = 35\,000$, and a variable number of cross-links, from CL = 7000 (upper dataset) down to CL = 2000 (lower dataset); see the legend. Whereas the effective rigidities for elastic storage decrease with the number of cross-links [as observed in experiments, (a)], all the calculated frictional losses fall within a common master curve compatible with the constant viscosity encoded in DPD-simulations (dashed line).

The *P. fluorescens* biofilms grown for 24 h under shaking conditions present higher shear moduli (both G' and G'', symbols in black) than those of a biofilm grown under static conditions (symbols in red), independently of the shear frequency probed in the linear regime of rheological response. Otherwise stated, the shaken biofilms develop higher rigidness than those grown under static conditions. Such Hookean stiffening is compatible with the nonlinear strengthening observed under stress (see Fig. 4). Culture shaking might constitute, indeed, a highly stressed biofilm growth setting, which elicits higher cross-linking than static growth, thus resulting into structural stiffening (so much as nonlinear stress results into effective dynamic strengthening). In general, the measured values of the storage modulus are found higher than the frictional losses (especially for low and intermediate frequencies when $G' > G''$). This is the typical behavior of soft solids displaying higher elastic resistance than frictional opposition to shear flow.[57] The observed rheological parsimony as a soft solid is characteristic for any *P. fluorescens* biofilm grown longer than 24 h (data not shown). For the biofilms grown under static conditions, the rheological experiments show, however, an increase in frictional losses at the highest frequencies tested, i.e., $G'' \sim \omega$ [see Fig. 7(a); dashed line]. This dissipative contribution leads to a viscoelastic inversion $G' \sim G''$, which is also characteristic for soft solids that strained at high rates make the viscous flow to emerge as a consequence of stress.[57] A similar behavior seems to be extrapolated in the shaken biofilm as far as the difference between G' and G'' becomes reduced upon increasing frictional losses at high frequencies, whereas the elastic storage remains constant [see Fig. 7(a)].

To test the capability of our synthetic biofilm model to capture experimental behavior in *P. fluorescens* biofilms, we perform numerical rheology, as reported in Fig. 7(b). After having explored the parameter space in Sec. III C, we choose to prepare a biofilm with the following parameters: $N_b = 184$, $N_p = 80$, $l_p = 100$, $N_s = 35\,000$, and $A = 75\%$, with a variable number of cross-links spanning the broad range $CL = 2000$–7000 (considered representative for poor and rich cross-linking, respectively, leading soft and stiff elasticity). As previously justified in Ref. 12, we assume, indeed, that the main difference between the biofilm grown under static and shaking conditions is only in the matrix composition, being one of the shaken-grown biofilms richer in cross-links.

Figure 7(b) plots the different datasets computed for G' (closed symbols) and G'' (hollow symbols) as a function of the frequency

of the shear strain imposed to the simulation box for the different number of cross-links in the chosen canonical T_A−topology. According to the established experimental conditions, we numerically compute the shear moduli of the DPD-model by changing the stress frequency over more than four orders of magnitude. Internal simulation units are converted into physical units according to the conversion factors previously described. Consistent with what we observed in experiments, G' softens with decreasing the number of cross-links but does not show a significant change upon increasing ω, corresponding to a soft solid with permanent cross-links unable to undergo relaxation.[54] Moreover, the computed values for the storage modulus (closed symbols) are systematically higher than the ones found for the loss modulus (hollow symbols), as expected for soft solids.[53] The numerical results in Fig. 7(b) refer to the T_A topology corresponding to the more open realization facilitating for bacterial reorganization. As previously shown in Fig. 2, these DPD-biofilms are spatially homogeneous in the microscopic terms revealed by the pair distribution function (PDF) structure. However, their rheological properties not only give consistent results when tested varying the parameter space (Fig. 6) but are also capable of qualitatively reproducing the high-frequency (small-scale) rheological behavior observed in experiments [Fig. 7(a)] even if they do not consider spatial inhomogeneity characteristic of real biofilms. Further work is in progress to explicitly mimic spatial inhomogeneities in the numerical DPD-based approach.

As expected, the simulated frictional losses markedly follow the dissipative particle dynamics as imprinted by the constant solvent viscosity in the whole frequency domain [i.e., $G'' = \omega\eta$; see Fig. 7(b)]. This marked unitary $G'' \approx \omega$ fingerprint actually corresponds to the intrinsic dissipation of the DPD-simulation method, which no longer operates as a collective relaxation in the largest mesoscopic scales (at low frequencies). This result is not only compatible with the Newtonian fluidity inherent to the microscopic-DPD but also agrees with what experimentally observed at high frequencies in both the stimulated shaken biofilms and the statically grown ones [although they do preserve the high frictional relaxation at low frequencies; see Fig. 7(a)]. However, the DPD-simulated values of G'' obtained at the lowest simulation frequencies appear more than two orders of magnitude smaller than G', which indicates a predominantly conservative mechanics under the *quasi*-static deformation conditions considered in simulations. The different simulated datasets fall indeed within a same master curve corresponding to a common viscous friction imparted by the solvent on the single structural entities (independently on the number of cross-links). The difference is progressively reduced upon increasing ω (increasing viscous friction under constant rigidity) up to the Newtonian flow behavior $G' \sim G'' = \eta\omega$ undergone by the synthetic DPD-biofilms at the higher simulated frequency (corresponding to the faster strain rates). A qualitatively similar behavior occurs in the experiments for *P. fluorescens* biofilms grown under static conditions albeit the difference between G' and G'' at low frequencies is not actually marked as predicted by simulations. These compared results validate, at least qualitatively, a synthetic capacity of our model DPD-biofilm for the predictive rheology in terms of permanent matrix cross-linking. Noticeably, no viscoelastic relaxation can be predicted as far as the cross-links remain fixed across the mapped scales.

IV. DISCUSSION

Biofilms are composed of bacteria that secrete a mesh of extracellular polymeric substances (EPSs) producing a viscoelastic matrix to which they eventually cross-link through complex (conservative and dissipative) mechanisms that result in a complex rheological response.[12–17] Even though a mathematical modeling of bacterial biofilms might provide a useful tool for controlling biofilm formation, up-to-date modeling cannot be considered completely satisfactory. Tailoring a detailed model that includes physical parameters to mimic hydrodynamics, solute mass transport and active dynamics of the bacterial population within the biofilm are indeed a challenging task. The parameterization of the individual components of a biofilm model increases the complexity of the algorithm beyond limited computational capacity.[58] Therefore, it would be highly desirable to design a structurally simplified model while retaining the relevant dynamics. Further including dynamical details arising from systemic memory effects could also be desirable although computationally unavoidable in the mesoscopic level of complexity requested to capture biofilm rheology as measurable in experiments.

By taking advantage of a Dissipative Particle Dynamics (DPD) simulation algorithm, we have validated a coarse-grained model of biofilm behavior to numerically explore the rheological properties of a *P. fluorescens* biofilm. The synthetic model is based on the DPD-approach depicted in Ref. 12 and consists of a topologically tunable simulation platform of permanent polymer chain cross-linking able to mimic a real bacterial biofilm approaching an effectively passive living component embedded with variable contents of EPS. Because DPD models allow us to simulate short range interactions of any statically embedded particle, our model enables for progressively increasing structural details at smaller spatial resolution in the polymerized (EPS) mesh, from the macroscopic scale of the rheological response, through the structural mesoscopic details down to the fluctuating behavior of the single particles under a detailed balance of thermal motion against frictional dissipation. This is an important advantage over the generally used long-range interaction models,[59] which are spatially limited by a continuous scale cutoff that impedes going deeper into smaller levels of detail, including the topology of cross-linking and the viscous friction in the underlying microscopic motions. Moreover, the "soft" nature of DPD-interactions allows us to increase the integration time by orders of magnitude, allowing us to explore rheological time scales normally inaccessible to atomistic simulations. However, our numerical DPD-simulation schema is only weakly dissipative (or too much "conservative") by only considering static permanent cross-linking different from real biofilms, including highly dissipative sinks and sources of mechanical energy, e.g., reconfigurable cross-links, sliding entanglements, and propulsive forces within the thriving bacteria. Therefore, our structurally simplified DPD-approach only captures essential features of linear mechanics but fails in describing the active nonlinear response observed in experiments. Whereas topologically static DPD-simulations naturally exhibit nonlinear strengthening due to chain ordering under large deformation, the real *P. fluorescens* biofilms used as a validating setting exhibit contradictory mechanical softening due to biological activities not considered in the current simulations.[12] Finally and foremost, our numerical DPD-algorithm explicitly includes hydrodynamics and thermal fluctuations, which are known to play a crucial role in introducing variability in

biological systems, such as the biofilms here considered.[60] Our modeling approach in essence simplifies the complexity of real biofilms, treating them as composite materials described by a set of physical parameters that recapitulate the principal ingredients of compositional and topological structures. The simulated DPD-biofilms have been constructed as a complex structure of the prescribed topology as fixed by the degree and density of cross-linking and the known composition by a class and number of interacting particles. Because of their mesoscopic nature, we have got access to simulate their rheological behavior dependent on the treatment processes imposing the history of the shear deformation in a way controlled by the dissipative frictional memory of the microscopic components.

We have chosen to study biofilms formed by *P. fluorescens* for three main reasons: (1) It is the same model system as explored in our previous study[12] and the other related ones, *P. aeruginosa* (see Ref. 15 for a recent review), making it easy to validate our simulation results with the already published ones (both experimental and numerical with a more limited scope). (2) DPD-simulations validated here allow us to make predictions in more extended spatiotemporal scales than conventional macro-rheological experiments do allow (including high frequencies and high strain rates often precluded by spurious inertial effects in experiments). (3) Although the model micro-organism used in this work for experimental validation of the simulation framework is non-pathogenic, other members of the genus *Pseudomonas* are often pathogenic, thus being requested for synthetic analysis *in silico*. As a relevant counterexample, *P. aeruginosa* is an opportunistic pathogen that is frequently associated with chronic biofilm infections, hence being attractive for simulation forecasting. Overall, the composition of the EPS is similar in both species, with a high proportion of acetylated polysaccharides (alginate-like) and extracellular DNA,[55,60] which suggests that the biofilm could be characterized by a similar mechanical behavior of *P. fluorescens*. The proposed DPD-simulations could make reasonable numerical forecasting on the physical biofilm's fate as performed in "digital tweens" for mechanical behavior, built *in silico* as synthetic biofilms resembling the mechanical properties of the real (pathogenic) biofilms.

V. CONCLUSIONS

By comparing the experimental and numerical results, we conclude that our proposed coarse-grained model qualitatively reproduces the behavior of rheological moduli over several decades of dynamic behavior. The measured elastic modulus was always higher than the loss modulus in both experiments and simulations corresponding to soft solid behavior.

Moreover, we predict the decreasing difference between G' and G'' observed at higher frequencies as a consequence of dominant viscous friction. This was clearly observed in the softer biofilms prepared under static conditions and predicted by DPD-simulations, including frictional dissipation as an essential dynamic ingredient. As a very characteristic feature of biofilm rheology, G' and G'' tended to converge for high frequency in both numerical and experimental outcomes. Nonetheless, simulations showed a larger dissipative gap between G' and G'' than what was observed in experiments. In general, when $G' \gg G''$, the system flows more like an inviscid liquid, whereas the regime where $G' \sim G''$ indicates a viscoelastic system. Hence, our DPD-model presents a marked transition from a rigid solid at low frequency toward a viscoelastic regime at higher frequencies. In the experiments with the real biofilms, this transition happens in a less pronounced way more compatible with a soft solid behavior over broader scales than in simulations.

The qualitative correspondence between real biofilms and synthetic DPD simulations endows the forecasting potential of using a coarse-grained DPD approach to biofilm rheology when modeling extremely complex biofilms. Even though the model strongly relies on an *a priori* detailed study of the parameter space, in future prospective, this will allow us to evaluate in more detail the biofilm transitions from a predominantly solid-like system to a predominantly liquid-like behavior through the interplay of the elastic and loss moduli upon changing the biofilm composition or growth conditions. In fact, this transition can be even more dramatic in biofilms prepared under static conditions and longer maturation times, where the elastic modulus vanishes at high frequency. We are currently working in this direction, studying how cross-linking dynamics may play a relevant role in these transitions.

As a prospective outlook, DPD-simulation knowledge on the dynamics of the mechanical transitions within synthetic biofilms may guide future strategies that allow for the penetration of antimicrobial agents into "soften" biofilm matrices, even predicting conditions for structural disassembly relevant for technological applications.

ACKNOWLEDGMENTS

B.O., I.L.-M., and C.V. acknowledge funding from Grant UCM/Santander PR26/16. C.V acknowledges funding from MINECO grants EUR2021-122001, PID2019-105343GB-I00, IHRC22/00002. F.M. acknowledges funding from MINECO under Grant Nos. PID2019-105606RB-I00, FIS2016-78847-P, PID2019-108391RB-I00, and FIS2015-70339; from the REACT-EU program PR38-21-28 ANTICIPA-CM, a grant by the Comunidad de Madrid and European Union under the FEDER Program; from EU in response to COVID-19 pandemics; and from Comunidad de Madrid under Grant Nos. S2018/NMT-4389 and Y2018/BIO-5207. C.V. acknowledges funding from MINECO under Grant No. PID2019-105343GB-I00. F.A acknowledges the support from the "Juan de la Cierva" program (Grant No. FJCI-2017-33580). A.K.M. is recipient of a Sara Borrell fellowship (Grant No. CD18/00206) financed by the Spanish Ministry of Health. V.B. acknowledges the support from the European Commission through Marie Skłodowska-Curie Fellowship No. 748170 ProFrost. Support from MINECO (Grant No. IRHC22/00002) is also acknowledged. The authors acknowledge the computer resources from the Red Española de Supercomputacion (RES) under Grant Nos. FI-2020-1-0015 and FI-2020-2-0032 and from the Vienna Scientific Cluster (VSC).

AUTHOR DECLARATIONS

Conflict of Interest

The authors have no conflicts to disclose.

Author Contributions

José Martín-Roca: Data curation (equal); Formal analysis (equal); Methodology (equal); Software (equal); Visualization (equal);

Writing – review & editing (lead). **Valentino Bianco**: Data curation (equal); Formal analysis (equal); Methodology (equal); Software (equal); Visualization (equal); Writing – review & editing (equal). **Francisco Alarcón**: Data curation (equal); Formal analysis (equal); Methodology (equal); Software (equal); Writing – review & editing (equal). **Ajay K. Monnappa**: Investigation (supporting); Writing – review & editing (supporting). **Paolo Natale**: Investigation (supporting); Writing – review & editing (equal). **Francisco Monroy**: Formal analysis (equal); Funding acquisition (equal); Investigation (equal); Methodology (equal); Writing – original draft (equal); Writing – review & editing (equal). **Belen Orgaz**: Conceptualization (lead); Funding acquisition (equal); Investigation (equal); Methodology (equal); Writing – original draft (equal); Writing – review & editing (equal). **Ivan López-Montero**: Conceptualization (lead); Formal analysis (equal); Funding acquisition (equal); Investigation (equal); Methodology (equal); Writing – original draft (equal); Writing – review & editing (equal). **Chantal Valeriani**: Conceptualization (lead); Formal analysis (equal); Funding acquisition (equal); Investigation (lead); Methodology (equal); Writing – original draft (equal); Writing – review & editing (lead).

DATA AVAILABILITY

The data that support the findings of this study are available from the corresponding author upon reasonable request.

REFERENCES

[1] B. W. Peterson, Y. He, Y. Ren, A. Zerdoum, M. R. Libera, P. K. Sharma, A.-J. van Winkelhoff, D. Neut, P. Stoodley, H. C. van der Mei, and H. J. Busscher, "Viscoelasticity of biofilms and their recalcitrance to mechanical and chemical challenges," FEMS Microbiol. Rev. **39**, 234–245 (2015).

[2] H.-C. Flemming and J. Wingender, J. Nat. Rev. Microbiol. **8**, 623 (2010).

[3] R. Donlan, Emerging Infect. Dis. **7**, 277 (2001).

[4] N. Høiby *et al.*, Int. J. Antimicrob. Agents **35**, 322 (2010).

[5] Z. Khatoon, C. D. McTiernan, E. J. Suuronen, T.-F. Mah, and E. I. Alarcon, "Bacterial biofilm formation on implantable devices and approaches to its treatment and prevention," Heliyon **4**, e01067 (2018).

[6] A. Milchev and K. Binder, "Adsorption of oligomers and polymers into a polymer brush formed from grafted ring polymers," Macromolecules **46**, 8724 (2013).

[7] J. Duan, S. Wu, X. Zhang, G. Huang, M. Du, and B. Hou, "Corrosion of carbon steel influenced by anaerobic biofilm in natural seawater," Electrochim. Acta **54**, 22–28 (2008).

[8] R. Mansour and A. Elshafei, "Role of microorganisms in corrosion induction and prevention," Br. Biotechnol. J. **14**, 1–11 (2016).

[9] M. P. Schultz and G. W. Swain, "The influence of biofilms on skin friction drag," Biofouling **15**, 129–139 (2000).

[10] B. R. Sveinbjörnsson, R. A. Weitekamp, G. M. Miyake, Y. Xia, H. A. Atwater, and R. H. Grubbs, "Rapid self-assembly of brush block copolymers to photonic crystals," Proc. Natl. Acad. Sci. U. S. A. **109**, 14332–14336 (2012).

[11] J. N. Wilking, T. E. Angelini, A. Seminara, M. P. Brenner, and D. A. Weitz, MRS Bull. **36**, 385 (2011).

[12] J. Jara, F. Alarcón, A. K. Monnappa, J. I. Santos, V. Bianco, P. Nie, M. P. Ciamarra, Á. Canales, L. Dinis, I. López-Montero, C. Valeriani, and B. Orgaz, Front. Microbiol. **11**, 588884 (2021).

[13] H. Boudarel, M. Jean-Denis, B. Blaysat, and M. Grediac, "Towards standardized mechanical characterization of microbial biofilms: Analysis and critical review," npj Biofilms Microbiomes **4**, 17 (2018).

[14] S. G. V. Charlton, M. A. White, S. Jana, L. E. Eland, P. G. Jayathilake, J. G. Burgess, J. Chen, A. Wipat, and T. P. Curtis, "Regulating, measuring, and modeling the viscoelasticity of bacterial biofilms," J. Bacteriol. **201**, e00101 (2019).

[15] S. Jana, S. G. V. Charlton, L. E. Eland, J. G. Burgess, A. Wipat, T. P. Curtis, and J. Chen, "Nonlinear rheological characteristics of single species bacterial biofilms," npj Biofilms Microbiomes **6**, 19 (2020).

[16] N. Billings, A. Birjiniuk, T. S. Samad, P. S. Doyle, and K. Ribbeck, "Material properties of biofilms—A review of methods for understanding permeability and mechanics," Rep. Prog. Phys. **78**, 036601 (2015).

[17] V. D. Gordon, M. Davis-Fields, K. Kovach, and C. A. Rodesney, "Biofilms and mechanics: A review of experimental techniques and findings," J. Phys. D: Appl. Phys. **50**, 223002 (2017).

[18] G. Klauck, D. O. Serra, A. Possling, and R. Hengge, "Spatial organization of different sigma factor activities and c-di-GMP signalling within the three-dimensional landscape of a bacterial biofilm," Open Biol. **8**, 180066 (2018).

[19] E. J. Stewart, M. Ganesan, J. G. Younger, and M. J. Solomon, "Artificial biofilms establish the role of matrix interactions in staphylococcal biofilm assembly and disassembly," Sci. Rep. **5**, 13081 (2015).

[20] M. Ganesan, E. J. Stewart, J. Szafranski, A. E. Satorius, J. G. Younger, and M. J. Solomon, "Molar mass, entanglement, and associations of the biofilm polysaccharide of staphylococcus epidermidis," Biomacromolecules **14**, 1474–1481 (2013).

[21] M. Vergara-Irigaray, J. Valle, N. Merino, C. Latasa, B. García, I. Ruiz de los Mozos, C. Solano, A. Toledo-Arana, J. R. Penadés, and I. Lasa, "Relevant role of fibronectin-binding proteins in staphylococcus aureus biofilm-associated foreign-body infections," Infect. Immun. **77**, 3978–3991 (2009).

[22] L. K. Jennings, K. M. Storek, H. E. Ledvina, C. Coulon, L. S. Marmont, I. Sadovskaya, P. R. Secor, B. S. Tseng, M. Scian, A. Filloux, D. J. Wozniak, P. L. Howell, and M. R. Parsek, "Pel is a cationic exopolysaccharide that cross-links extracellular DNA in the *Pseudomonas aeruginosa* biofilm matrix," Proc. Natl. Acad. Sci. U. S. A. **112**, 11353–11358 (2015).

[23] J. Sankaran, A. Karampatzakis, S. A. Rice, and T. Wohland, "Quantitative imaging and spectroscopic technologies for microbiology," FEMS Microbiol. Lett. **365**, fny075 (2018).

[24] M. Tallawi, M. Opitz, and O. Lieleg, "Modulation of the mechanical properties of bacterial biofilms in response to environmental challenges," Biomater. Sci. **5**, 887–900 (2017).

[25] E. S. Gloag, G. K. German, P. Stoodley, and D. J. Wozniak, "Viscoelastic properties of *Pseudomonas aeruginosa* variant biofilms," Sci. Rep. **8**, 9691 (2018).

[26] I. Klapper and J. Dockery, SIAM Rev. **52**, 221 (2010).

[27] M. Wang and M. Thanou, "Targeting nanoparticles to cancer," Pharmacol. Res. **62**, 90–99 (2010).

[28] T. Zhang, N. G. Cogan, and Q. Wang, SIAM J. Appl. Math. **69**, 641 (2008).

[29] N. Kandemir, W. Vollmer, N. S. Jakubovics, and J. Chen, Sci. Rep. **8**, 10893 (2018).

[30] C. Picioreanu, M. C. M. van Loosdrecht, and J. J. Heijnen, Water Sci. Technol. **39**, 115 (1999).

[31] C. Picioreanu, J.-U. Kreft, and M. C. M. van Loosdrecht, Appl. Environ. Microbiol. **70**, 3024 (2004).

[32] R. D. Groot and P. B. Warren, "Dissipative particle dynamics: Bridging the gap between atomistic and mesoscopic simulation," J. Chem. Phys. **107**, 4423–4435 (1997).

[33] P. Español and P. B. Warren, "Perspective: Dissipative particle dynamics," J. Chem. Phys. **146**, 150901 (2017).

[34] C. Peskin and D. M. McQueen, J. Comput. Phys. **81**, 372 (1977).

[35] C. S. Peskin, Acta Numer. **11**, 479 (2002).

[36] J. F. Hammond, E. J. Stewart, J. G. Younger, M. J. Solomon, and D. M. Bortz, Comput. Model. Eng. Sci. **98**, 295 (2014).

[37] J. A. Stotsky, J. F. Hammond, L. Pavlovsky, E. J. Stewart, J. G. Younger, M. J. Solomon, and D. M. Bortz, J. Comput. Phys. **317**, 204 (2016).

[38] H. Horn and S. Lackner, Adv. Biochem. Eng./Biotechnol. **146**, 53 (2014).

[39] H. J. Eberl *et al.*, "Computing intensive simulations in biofilm modeling," in *22nd International Symposium on High Performance Computing Systems and Applications* (IEEE, 2008).

[40] Y. Liu and A. C. Balazs, Langmuir **34**, 1807 (2018).

[41] L. Xu, N. Giovambattista, S. V. Buldyrev, P. G. Debenedetti, and H. E. Stanley, "Waterlike glass polyamorphism in a monoatomic isotropic Jagla model," J. Chem. Phys. **134**, 064507–064514 (2011).

[42]M. Bol *et al.*, Crit. Rev. Biotechnol. **33**, 145 (2012).
[43]G. Raos and M. Casalegno, J. Chem. Phys. **134**, 054902 (2011).
[44]M. Mukhi and A. Vishwanathan, "Identifying potential inhibitors of biofilm-antagonistic proteins to promote biofilm formation: A virtual screening and molecular dynamics simulations approach," Mol. Diversity **26**, 2135 (2021).
[45]Z. Xu, P. Meakin, A. Tartakovsky, and T. D. Scheibe, "Dissipative-particle-dynamics model of biofilm growth," Phys. Rev. E **83**, 066702 (2011).
[46]P. Barai, A. Kumar, and P. P. Mukherjee, "Modeling of mesoscale variability in biofilm shear behavior," PLoS One **11**, e0165593 (2016).
[47]L. Pavlovsky, J. G. Younger, and M. J. Solomon, "In situ rheology of staphylococcus epidermidis bacterial biofilms," Soft Matter **9**, 122–131 (2013).
[48]J. A. Stotsky, V. Dukic, and D. M. Bortz, Eur. J. Appl. Math. **29**, 1141 (2018).
[49]G. Raos, M. Moreno, and S. Elli, "Computational experiments on filled rubber viscoelasticity: What is the role of particle–particle interactions?," Macromolecules **39**, 6744–6751 (2006).
[50]S. Plimpton, "Fast parallel algorithms for short-range molecular dynamics," J. Comput. Phys. **117**, 1–19 (1995).
[51]P. J. Hoogerbrugge and J. M. V. A. Koelman, Europhys. Lett. **19**, 155 (1992).
[52]G. Alonci, F. Fiorini, P. Riva, F. Monroy, I. López-Montero, S. Perretta, and L. De Cola, "Injectable hybrid hydrogels, with cell-responsive degradation, for tumor resection," ACS Appl. Bio Mater. **1**, 1301–1310 (2018).
[53]W. N. Findley and F. A. Davis, *Creep and Relaxation of Nonlinear Viscoelastic Materials* (Courier Corporation, 2013).
[54]A. Aufderhorst-Roberts and G. H. Koenderink, "Stiffening and inelastic fluidization in vimentin intermediate filament networks," Soft Matter **15**, 7127–7136 (2019).
[55]J. Kives, B. Orgaz, and C. SanJosé, "Polysaccharide differences between planktonic and biofilm-associated EPS from *Pseudomonas fluorescens* B52," Colloids Surf. B **52**, 123 (2006).
[56]M. S. Waters, S. Kundu, N. Lin, and S. Lin-Gobson, "Microstructure and mechanical properties of *in situ Streptococcus mutans* biofilms," ACS Appl. Mater. Interfaces **6**(1), 327–332.
[57]F. Fiorini, E. A. Prasetyanto, F. Taraballi, L. Pandolfi, F. Monroy, I. López-Montero, E. Tasciotti, and L. De Cola, "Nanocomposite hydrogels as platform for cells growth, proliferation, and chemotaxis," Small **12**, 4881–4893 (2016).
[58]C. S. Calude and G. Longo, "The deluge of spurious correlations in big data," Found. Sci. **22**, 595–612 (2017).
[59]R. D. Groot, "Applications of dissipative particle dynamics," in *Novel Methods in Soft Matter Simulations* (Springer, 2004), pp. 5–38.
[60]M. Krsmanovic, D. Biswas, H. Ali, A. Kumar, R. Ghosh, and A. K. Dickerson, "Hydrodynamics and surface properties influence biofilm proliferation," Adv. Colloid Interface Sci. **288**, 102336 (2021).